

Nonlinear optical bistability in microring resonators for enhanced phase sensing

Patrick Tritschler,^{*} Christian Schweikert,[†] Rouven H. Klenk,[†] Simon Abdani,[†] Onur Sözen,[†] Wolfgang Vogel,[†] Georg Rademacher,[†] Torsten Ohms,[‡] André Zimmermann,[§] and Peter Degenfeld-Schonburg[¶]

(Dated: August 13, 2024)

Photonic microring resonators are used in a variety of chip-integrated sensing applications where they allow to measure transmission intensity changes upon external signals with a sensitivity that scales linearly with the Q-factor. In this work, we suggest to exploit the nonlinear self-phase-modulation effect to increase the overall sensitivity by an additional gain factor appearing when the operational point of the nonlinear resonator is chosen just at the cross-over from the mono- to the bistable regime. We present the theoretical idea together with a first proof of concept experiment displaying a gain factor of 22 on a chip-integrated silicon-nitride resonator.

I. INTRODUCTION

Microring resonators are one of the most popular optical chip-integrated components. They have served for many fundamental investigations and pushed a vast number of technological advances [1–8]. In the simplest form they consist of a ring-shaped waveguide which is within the range of the evanescent light field to a straight waveguide as illustrated in Fig. 1. Ring resonators are used in many various applications like optical filters [9–11], optical bio sensors [7, 12–15], frequency comb generation [3, 4], squeezed light generation for sensing applications [16, 17], optical phase sensors and many more.

In the following, we focus on optical phase sensors like they are used for example in ring-gyroscopes, where the Sagnac effect changes the effective path length [18–20], or optical temperature sensors, where a temperature influence affects the ring-geometry [21–23]. In both applications the optical phase and thus the resonance condition of the ring resonator is effectively changed, which also affects the output transmission power. In order to increase the sensitivity of the transmitted power with respect to a phase shift, it is necessary to increase the quality factor of the resonator by optimizing the fabrication process of the photonic devices [2, 20, 24].

In this work, we propose to utilize the nonlinear self-phase modulation (SPM) effect to achieve a sensitivity improvement over the linear resonator operation via a multiplicative nonlinear gain factor larger than one. The SPM effect occurs whenever the pump power and therefore the field inside the resonator is large enough to enter

the nonlinear regime. Here, the nonlinear optical or thermal processes lead to the tilting of the resonance curve which even ends up in the well-known optical bistability for large enough pump power [25]. The largest slope of the resonance curve, and thus the largest nonlinear gain factor, appears when the operational point of the nonlinear resonator is chosen just at the cross-over from the monostable to the bistable regime. We give a clear theoretical picture of how the operational point of the nonlinear resonator, also known as the Duffing or Kerr oscillator [26, 27], can be chosen in order to be at the sweet spot which can lead to nonlinear gain factors by far exceeding unity.

The self-heating effect in microring resonators, which leads to an SPM effect, has already been discussed in detail for chip-integrated applications, with a successful modeling in different material platforms [23, 28–35]. Furthermore, the SPM effect can also originate from optical four-wave mixing induced by the $\chi^{(3)}$ nonlinearity and the combination of both effects were investigated in [36, 37]. Therefore, we experimentally characterize the thermal and optical properties of our resonator consisting of a silicon nitride (Si3N4) ring and show the increase of the sensitivity in accordance with the theoretical expectation. By placing a metal-heater above the ring resonator we applied a temperature change to represent a phase shift which allowed us to measure the sensitivity improvement with a nonlinear gain factor of up to 22. The agreement of the results to the theoretical model gives us the confidence that with a proper electronic control loop and thus with a much better control of the system parameters at the sweet-spot, even gain factors of up to 100 or higher are achievable.

This paper is structured as follows. First, the ring resonator for the application of phase sensing is discussed in chapter II. The classical equations of motion to describe our system and its thermal modelling are introduced in sections II A and II B which are followed by the discussion of the sensitivity boost in section II C. Afterwards, the experimental setup is presented in chapter III followed by the results in chapter IV. We conclude with a discussion and a summary in chapter V and VI, respectively.

^{*} patrick.tritschler@bosch-sensortec.com; Bosch Sensortec GmbH, Gerhard-Kindler Straße 9, Reutlingen, 72770, Germany; Institute for Micro Integration (IFM), University of Stuttgart, Allmandring 9b, Stuttgart, 70569, Germany

[†] Institute of Electrical and Optical Communications, Pfaffenwaldring 47, 70569 Stuttgart, Germany

[‡] Bosch Sensortec GmbH, Gerhard-Kindler Straße 9, Reutlingen, 72770, Germany

[§] University of Stuttgart, Institute for Micro Integration (IFM) and Hahn-Schickard, Allmandring 9b, Stuttgart, 70569, Germany

[¶] Robert Bosch GmbH, Robert-Bosch-Campus 1, Renningen, 71272, Germany

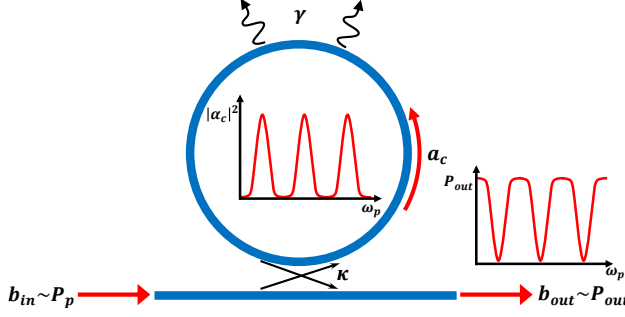


Figure 1. Schematic setup of a microring resonator.

II. NONLINEAR MICRORING RESONATOR FOR PHASE SENSING

In the following we introduce our model of a single nonlinear optical mode inside of a ring resonator as sketched in Fig. 1. An external input laser provides the optical power P_p in the straight waveguide with the amplitude $b_{\text{in}} = \sqrt{P_p/\hbar\omega_p}$ and the angular frequency ω_p to pump the ring. At a reference temperature T_0 , the modes inside the ring resonator have angular resonance frequencies at $\omega_{R,T_0} = 2\pi c m/n_{\text{eff}} L_{\text{eff}}$ with the speed of light c in vacuum, the mode index $m = 1, 2, \dots$, the effective refractive index n_{eff} and the effective resonator length L_{eff} [38]. In the following section we first describe the optical behavior, proceed with the thermal influences and conclude with the application for phase sensing.

A. Classical dynamics of a nonlinear optical mode

For our investigations it suffices to describe a single optical mode by its classical equations of motion within rotating-wave approximation [16, 25]

$$\frac{d}{dt}\alpha_c = (i\Delta_{\text{tot}} - \Gamma)\alpha_c + \sqrt{\kappa}b_{\text{in}}. \quad (1)$$

Here, α_c describes the dimensionless classical amplitude of the optical field a_c inside the ring resonator in a rotating frame of the pump frequency ω_p . The rate κ describes the coupling efficiency between the waveguide and the ring, while the loss rate γ includes all losses appearing in the ring which are summed up to the total losses $\Gamma = \kappa + \gamma$. The overall detuning between the pump frequency and the effective resonance frequency of the optical mode is given by

$$\Delta_{\text{tot}} = \omega_p - \omega_{R,T_0} + g_{\text{tot}}|\alpha_c|^2 + \omega_{R,T_0}a_{\text{th}}\Delta T_{\text{ext}} \quad (2)$$

The nonlinearity of Eq.(1) appears in the detuning which depends on the photon number $|\alpha_c|^2$. This is known as the Kerr or SPM effect and it becomes relevant when the photon number $|\alpha_c|^2$ is on the order of $\sim \omega_{R,T_0}/(g_{\text{tot}}Q)$ with the quality factor of the resonator defined by $Q =$

$\omega_{R,T_0}/\Gamma$. The total gain factor $g_{\text{tot}} = g_{\text{opt}} + g_{\text{th}}$ includes the optical contribution g_{opt} which originates from the small but finite $\chi^{(3)}$ nonlinearity of silicon-nitride. It can be either extracted from a frequency comb measurement [39] or directly calculated by using a quantitative value for the nonlinear refractive index [16]. Finally, the detuning contains contributions from thermal effects leading to both a thermal gain factor g_{th} and to a thermally induced phase shift $\omega_{R,T_0}a_{\text{th}}\Delta T_{\text{ext}}$ which we will discuss in the following subsection.

B. Thermal modeling

Under temperature changes $\Delta T = T - T_0$ upon the ring resonator, the effective index as well as the geometric length of the resonator change, which leads to a shift of the angular resonance frequency according to $\omega_{R,T}(T) = \omega_{R,T_0} - \omega_{R,T_0} \cdot a_{\text{th}}\Delta T$, with the temperature coefficient $a_{\text{th}} = \frac{1}{L_{\text{eff}}} \frac{dL_{\text{eff}}}{dT} + \frac{1}{n_{\text{eff}}} \frac{dn_{\text{eff}}}{dT}$ [28]. The temperature coefficient describes the thermal expansion as well as the change of the effective refractive index and depends on the used material and geometry. However, in addition to externally induced temperature changes resulting in a finite ΔT , also self-heating causes a change of the angular resonance frequency. In this case, an optical field inside the resonator can be absorbed by the waveguide material and leads to a heating of the system due to different inelastic photon-phonon interaction processes like surface state absorption which also appears in Si_3N_4 ring resonators [40, 41] such as the one used in our experiment. The well-known relaxation dynamics [29, 42] of the internal temperature change ΔT_{int} caused by self-heating is described by thermal diffusion $\frac{d}{dt}\Delta T_{\text{int}}(t) = \delta_{\text{th}}\hbar\omega_p|\alpha_c|^2 - \gamma_{\text{th}}\Delta T_{\text{int}}(t)$ with the absorption rate δ_{th} and the thermal relaxation rate γ_{th} . A further detailed derivation can be found in appendix A but it is important to mention that the relaxation time of our ring resonator is on the order of μs . Thus, all our experimental investigation where performed giving the system enough time to relax into the steady state. Furthermore, the internal temperature change is always proportional to the photon number $|\alpha_c|^2$ leading to the thermal SPM effect. By introducing the external temperature change ΔT_{ext} with $\Delta T = \Delta T_{\text{ext}} + \Delta T_{\text{int}}$, we end up with the thermal terms for the total detuning Δ_{tot} introduced in Eq. 2.

C. Sensitivity boost by the nonlinear gain factor

Next, we investigate the potential for enhancing the sensitivity of phase sensing applications by exploiting the tilting of the transmission measurement caused by the SPM effect. The conceptual idea can be understood using the steady state output transmission curves $T = P_{\text{out}}/P_p$ over the wavelength detuning $\lambda_p - \lambda_R$, with $\lambda_p = 2\pi c/\omega_p$ and $\lambda_R = 2\pi c/\omega_{R,T_0}$ for different pump amplitudes as shown in Fig. 2. The sensitivity of our

sensing concept is directly given by the slope of the transmission curve as an external phase shift would cause a change of the resonance frequency and thus a change of the output transmission. The steady state output power $P_{\text{out}} \equiv |b_{\text{out}}^{ss}|^2$ is obtained from the classical input-output relation $b_{\text{out}}^{ss} = \sqrt{\kappa} \alpha_c^{ss} - b_{\text{in}}$, with the steady state field amplitude $\alpha_c^{ss} = \lim_{t \rightarrow \infty} \alpha_c(t)$. The latter is obtained by solving Eq. 1, which however defies a simple analytical expression due to the nonlinear SPM effect as shown in more details in appendix B.

Nonetheless, we are able to put simple analytical insights for all the quantities that are required within our conceptual idea. First of all, we have the power

$$P_{\text{max}} = \frac{\sqrt{3} \hbar \omega_p \Gamma^3}{9 g_{\text{tot}} \kappa} \quad (3)$$

which marks the cross-over from the monostable to the bistable regime. Our sensing scheme will work best slightly below P_{max} and break down in the bistable regime. We find that the point of maximal slope of the transmission curve is always at a frequency detuning of $\Delta_{\text{opt}} = -3g_{\text{tot}}\kappa P_p / \Gamma^2 \hbar \omega_p - \Gamma / \sqrt{12}$ with $\Delta_{\text{opt}} = \omega_p - \omega_{R,T_0}$. Finally, as shown in more detail in appendix C, the phase sensitivity of the ring resonators output upon an external frequency change in W/Hz is given by

$$S = S_{\text{lin}} \cdot \frac{P_{\text{max}}}{P_{\text{max}} - P_p} \quad (4)$$

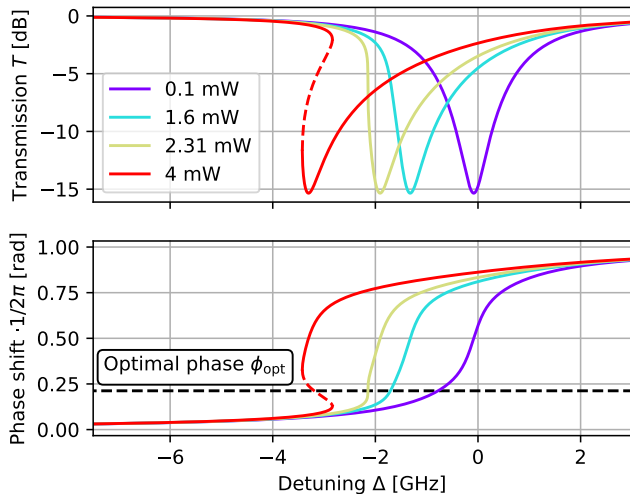


Figure 2. **Top:** Modeled output transmission for different input powers using equation C1 from appendix C. The blue line shows the linear case at small input power, orange shows the case below P_{max} in the monostable regime, while green shows the case at P_{max} , thus just at the cross-over from the monostable to the bistable regime, and the red line shows the case above P_{max} where optical bistability occurs. **Bottom:** Phase shift of the transmitted light for different input powers highlighting the pump power independent optimal phase at which the transmission curve has the steepest slope.

with $S_{\text{lin}} = -\sqrt{27} P_p Q [1/4 - (\kappa/\Gamma - 1/2)^2] / \omega_{R,T_0}$. As expected, the linear sensitivity S_{lin} scales linearly with the pump power P_p and the quality factor of the resonator. Moreover, it is desired to design the ring resonator system close to the so called critical coupling point [43] where $\kappa \approx \gamma$ in order to maximize the sensitivity. In contrast to the linear resonator concept, the sensitivity will be boosted by a multiplicative gain factor $G = P_{\text{max}} / (P_{\text{max}} - P_p)$ in our nonlinear resonator concept. If P_p is close to P_{max} , then a large nonlinear gain can be achieved. It is clearly visible in equation 3 and 4 that a high g_{tot} results in a lower P_{max} and thus in a larger sensitivity at lower P_p .

III. EXPERIMENTAL SETUP

To validate the derived equations and to show the potential of our concept, we designed and characterized a chip-integrated Si_3N_4 ring resonator. The ring consists of a waveguide with a height of 800 nm, a width of 1.6 μm , a length of 1319.46 μm and a gap between the ring and the straight waveguide of 0.52 μm . The optical waveguide is surrounded by silicon dioxide (SiO_2). Starting from a tuneable laser source with a center wavelength of 1550 nm, the laser light is coupled via optical fibers to a polarization controller. This is followed by an optical amplifier, an optical attenuator and finally, the laser light is coupled into the chip by edge coupling via lensed fibers. The schematic of the experimental setup and an image of our ring resonator are shown in Fig. 3. By using the amplifier, a constant optical power is set and adjusted by the attenuator. This ensures that a polarization set by the polarization controller remains constant as the power varies. The light in the optical chip couples from the straight waveguide into the ring resonator and the out-coupled light is collected together with the transmitted one via edge coupling and then sent to an optical power meter which forms the detector stage. The optical power is measured before and after the chip to determine the coupling losses of the system. A metal-heater is placed above the ring resonator and is connected to a voltage controller to be able to change the temperature of the ring. By using this heater, the resonance frequency ω_{R,T_0} can be influenced with an applied temperature shift and represents a possible phase shift to mimic an external phase shift which we exploit to measure the sensitivity of our setup. For an additional thermal characterization, a Peltier-element is placed below the micro-chip to be able to apply an accurate temperature change to the whole chip for further characterization.

IV. RESULTS

First, we vary the temperature and measure the transmitted power to characterize the thermal properties of the ring resonator. Therefore, we set a fix tempera-

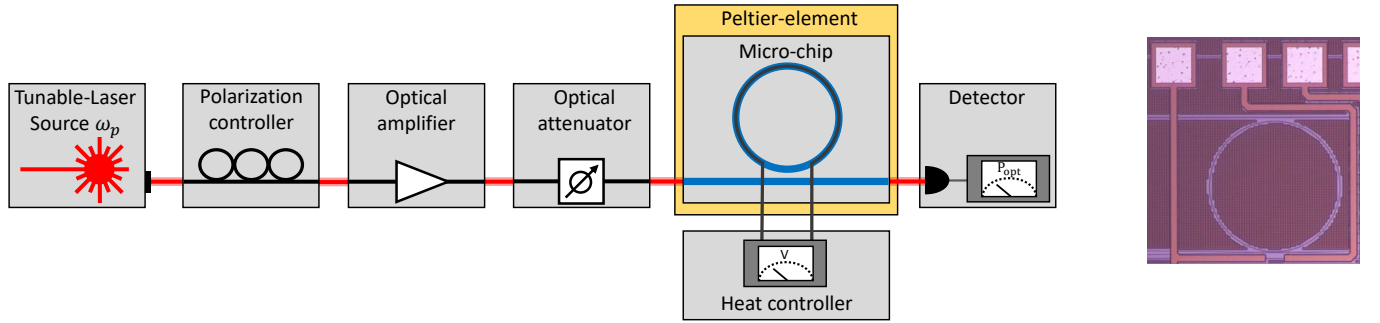


Figure 3. **Left:** Schematic of the measurement setup. **Right:** Image of the used microring resonator structure with a metal-heater layer on top.

ture by the Peltier-element and vary it to measure the change of the resonance frequency from which we identify $a_{th} = 1.226 \cdot 10^{-5} \text{ 1/K}$.

Next, we perform transmission measurements starting from a low optical power inside the straight waveguide with $P_p = 0.40 \text{ mW}$ to characterize the linear behavior from which we deduce the coupling rate $\kappa = 1450.64 \text{ MHz}$ as well as the loss rate to $\gamma = 1027.42 \text{ MHz}$ from the classical input-output theory which is shown in Eq. C1 in the appendix. This leads to a ring resonator Q-factor of $4.9 \cdot 10^5$. Then, we increase the power up to where the bistability appears and use the transmission curves to extract a total gain factor of $g_{\text{tot}} \approx 112 \text{ Hz}$. The optical gain factor is calculated to $g_{\text{opt}} \approx 2 \text{ Hz}$, which leads to $g_{\text{th}} \approx 110 \text{ Hz}$ and this shows that self-heating is the dominant process over the optical SPM effect. The measurement results and the calculations using the extracted parameter values are shown as dots and lines in Fig. 4, respectively. The tilting of the transmission spectrum and a bistability at increased input power is clearly visible while the theoretical model matches well with the measurements.

To demonstrate the sensitivity improvement by utilizing the SPM effect, we perform sensitivity measurements for different input powers while keeping P_p below P_{max} which using the extracted parameter values results in $P_{\text{max}} = 2.31 \text{ mW}$. For this purpose, we set the wavelength of the pump laser to match the optimal detuning Δ_{opt} for each pump power and applied additional small phase shifts using the metal heater above the ring resonator. Finally, we measured the change of the optical output power to determine the sensitivity S . The results are shown in Fig. 5. Each value at various input power P_p is normalized to the measurement result at a small input power with the reference sensitivity S_0 which corresponds to the linear resonance curve. It can be seen that the sensitivity rises with an increasing input power. Clearly, the measurement results follow the trend of the sensitivity as predicted by the theoretical model with equation 4. Additionally, the linear trend is shown as a reference. We will discuss the deviation of the measured results from the theoretical predictions in the next section.

V. DISCUSSION

The results displayed in Fig. 5 show an sensitivity improvement factor of up to 22.6 in contrast to the reference sensitivity S_0 in the linear operation limit of the ring resonator. Note, that we only managed to properly measure the slope of the transmission curves for input powers of up to 1.9 mW which corresponds to only 80 % of the maximal power $P_{\text{max}} \approx 2.3 \text{ mW}$. This is due to the fact that with our setup we were only able to resolve the detuning between the pump wavelength and the effective resonance wavelength of the cavity with an accuracy of 0.1 pm. We expect that with a higher resolution both, the matching between the theoretical model and the experimental data, and the overall nonlinear gain factor will be much more convincing.

Moreover, we have found that the phase shift between the input laser light and the output light is independent of the input power and constant at the optimal frequency

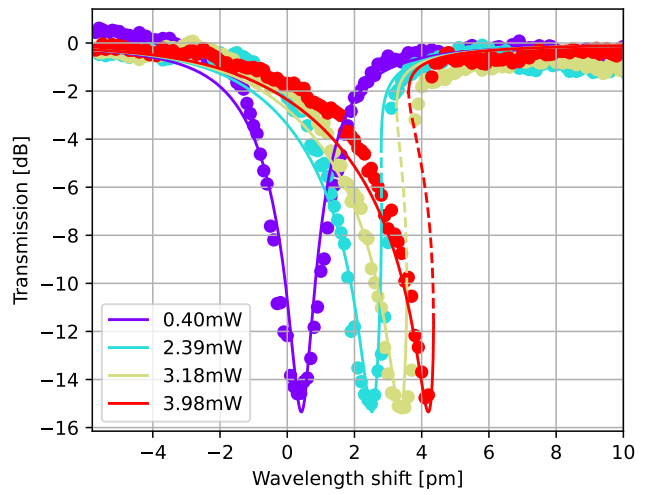


Figure 4. Optical bistability measurements (dots) and the theoretical model using the experimentally determined parameters (lines).

detuning Δ_{opt} , see also Fig 2. At Δ_{opt} the phase shift is given by

$$\phi_{\text{opt}} = -i \log \left(-\frac{2\Gamma - 3\kappa + \sqrt{3}i\kappa}{\sqrt{3\kappa^2 + (2\Gamma - 3\kappa)^2}} \right) + \pi. \quad (5)$$

Therefore, one can use an electronic control loop to find the laser frequency or rather wavelength which fulfills the phase shift ϕ_{opt} to be just at the optimal operational point of steepest slope and thus highest sensitivity. If these measures are all implemented, we expect that non-linear gain factors of up to 100 or even higher are achievable.

VI. SUMMARY

In this work we demonstrate the possibility of using the tilting of the transmission measurement caused by the SPM effect to increase the sensitivity of a ring resonator for phase sensing applications. We introduced the theoretical concept on a single optical mode with a Kerr and self-heating nonlinearity and validated our model by measurements on a chip-integrated Si_3N_4 ring resonator where we have been able to prove a sensitivity improvement factor of around 22 experimentally.

However, our sensing concept gives the perspective that with a well-suited control loop sensitivity improvement factors of more than 100 are achievable. Thus, our work addresses many phase sensing applications such as temperature sensors, biosensors, and optical gyroscopes.

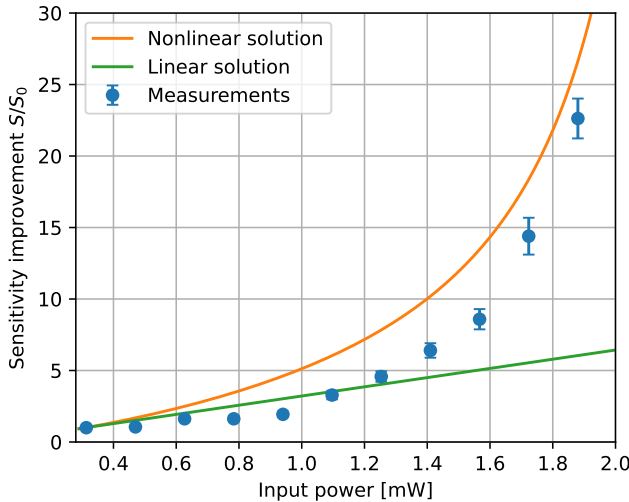


Figure 5. Sensitivity measurements (blue), the modeled expectation for the linear model (green) and the nonlinear model according to Eq. 4 (orange).

ACKNOWLEDGMENTS

The IPCEI ME/CT project is supported by the Federal Ministry for Economic Affairs and Climate Action on the basis of a decision by the German Parliament, by the Ministry for Economic Affairs, Labor and Tourism of Baden-Württemberg based on a decision of the State Parliament of Baden-Württemberg, the Free State of Saxony on the basis of the budget adopted by the Saxon State Parliament, the Bavarian State Ministry for Economic Affairs, Regional Development and Energy and financed by the European Union - NextGenerationEU.

Appendix A: Thermal modeling

In this appendix we derive the detuning Δ_{tot} for the main text in more detail which is required to model the SPM effect. If temperature is applied to the ring resonator, then the effective index as well as the geometric length of the resonator changes, which leads to a shift of the angular resonance frequency. Following [29, 42], we start with the equation of thermal diffusion to describe the dynamics of the internal temperature change ΔT_{int} caused by self-heating inside the ring resonator with

$$\frac{d}{dt} \Delta T_{\text{int}}(t) = \delta_{\text{th}} \hbar \omega_p |a_c|^2 - \gamma_{\text{th}} \Delta T_{\text{int}}(t). \quad (\text{A1})$$

Here, the thermal relaxation rate γ_{th} corresponds to the heat equalization with the environment and the thermal absorption rate δ_{th} describes the self-heating of the ring resonator. The thermal absorption rate is given by

$$\delta_{\text{th}} = \frac{2n_{\text{eff}} \gamma_{\text{abs}}}{c_p \rho A_{\text{eff}} L_{\text{eff}}}, \quad (\text{A2})$$

with the specific heat capacity c_p , mass density ρ and the loss rate γ_{abs} that depends on the absorption losses α_{abs} with [23]

$$\gamma_{\text{abs}} = \frac{(1 - e^{-\alpha_{\text{abs}} L_{\text{eff}}}) c}{n_{\text{eff}} L_{\text{eff}}} \quad (\text{A3})$$

The thermal relaxation rate γ_{th} depends on the thermal capacity $C_{\text{th}} = \rho c_p V$ and the thermal resistance which can be approximated for a rectangular waveguide to $R_{\text{th}} = 1/4kL_{\text{eff}}$ with the thermal conductivity k and the waveguide volume V [29, 42, 44]. Using $A_{\text{eff}} \approx V/L_{\text{eff}}$ we get

$$\gamma_{\text{th}} = \frac{1}{\tau_{\text{th}}} = \frac{1}{R_{\text{th}} C_{\text{th}}} = \frac{4k}{\rho c_p A_{\text{eff}}}. \quad (\text{A4})$$

which in our work results to the thermal relaxation time $\tau_{\text{th}} \approx 0.5 \mu\text{s}$. It is important to note that a correct assumption for γ_{th} is not possible using only the values of the optical waveguide due to the complex interaction between the ring resonator and the materials around it. Instead, a better approximation is achieved by using the

box material for k , as the material around the optical waveguide plays a crucial role in heat dissipation [35]. Solving equation A1 for the steady state leads to

$$\Delta T_{\text{int}} = \frac{\delta_{\text{th}} \hbar \omega_p}{\gamma_{\text{th}}} |a_c|^2 = \frac{n_{\text{eff}} \gamma_{\text{abs}} \hbar \omega_p}{2k L_{\text{eff}}} |a_c|^2. \quad (\text{A5})$$

The thermal detuning can be introduced using this result, the definition of an external temperature change ΔT_{ext} with $\Delta T = \Delta T_{\text{ext}} + \Delta T_{\text{int}}$ as

$$\Delta_{\text{th}} = \omega_p - \omega_{R,T_0} + \omega_{R,T_0} a_{\text{th}} \Delta T_{\text{ext}} + g_{\text{th}} |a_c|^2 \quad (\text{A6})$$

with the the thermal gain

$$g_{\text{th}} = \frac{\delta_{\text{th}} \hbar \omega_p a_{\text{th}} \omega_{R,T_0}}{\gamma_{\text{th}}} \approx \frac{\hbar \omega_p^2 n_{\text{eff}} \gamma_{\text{abs}} a_{\text{th}}}{2k L_{\text{eff}}}. \quad (\text{A7})$$

Finally, combining the optical and the thermal detuning leads to the total detuning which includes both influences as

$$\Delta_{\text{tot}} = \omega_p - \omega_{R,T_0} + g_{\text{opt}} |a_c|^2 + g_{\text{th}} |a_c|^2 + \omega_{R,T_0} a_{\text{th}} \Delta T_{\text{ext}} \quad (\text{A8})$$

The optical nonlinearity is defined as

$$g_{\text{opt}} \approx \frac{\hbar \omega_p^2 v_g^2 n_2}{c A_{\text{eff}} L_{\text{eff}}}, \quad (\text{A9})$$

with the group velocity v_g , the effective mode area A_{eff} and the nonlinear refractive index n_2 [16, 45].

Appendix B: Cavity power

To derive the equations in the main text, we start by describing the steady state field amplitude inside of the resonator α_c^{ss} . Using equation 1 of the main text with Δ_{tot} for the detuning, we can introduce three dimensionless parameters for the cavity field A , the pump field B and the detuning δ with the definitions

$$|A|^2 = \frac{g_{\text{tot}}}{\Gamma} |a_c|^2, \quad (\text{B1})$$

$$|B|^2 = \frac{g_{\text{tot}}}{\Gamma^3} \kappa |b_{\text{in}}|^2, \quad (\text{B2})$$

$$\delta = \frac{\Delta_{\text{tot}}}{\Gamma} = \frac{\Delta_{\text{lin}}}{\Gamma} + \frac{g_{\text{tot}}}{\Gamma} |a_c|^2 = \tilde{\delta} + |A|^2. \quad (\text{B3})$$

Thereby, $g_{\text{tot}} = g_{\text{th}} + g_{\text{opt}}$ is the total nonlinear gain and $\Delta_{\text{lin}} = \omega_p - \omega_{R,T_0} + \omega_{R,T_0} a_{\text{th}} \Delta T_{\text{ext}}$ the linear detuning with $\tilde{\delta} = \Delta_{\text{lin}}/\Gamma$. This leads to the following dimensionless description of the field inside of the ring resonator

$$|A|^2 = \frac{|B|^2}{\frac{1}{4} + (\tilde{\delta} + |A|^2)^2}. \quad (\text{B4})$$

The motivation for the dimensionless description is that this leads to simpler solutions that only depend on B

and $\tilde{\delta}$. Solving equation B4 for $|A|^2$ leads to one physical solution for the input power at $|B|^2 \leq \sqrt{3}/9$ given by

$$|A|^2 = \frac{3 - \left(2\tilde{\delta} + \sqrt[3]{\Xi} \right)^2}{6\sqrt[3]{\Xi}} \quad (\text{B5})$$

with

$$\Xi = -8\tilde{\delta}^3 - 18\tilde{\delta} - 108B^2 + 3\sqrt{3} \cdot \sqrt{16\tilde{\delta}^4 + 64\tilde{\delta}^3 B^2 + 8\tilde{\delta}^2 + 144\tilde{\delta} B^2 + 432B^4 + 1}. \quad (\text{B6})$$

The cross-over from the monostable to the bistable regime is marked by $|B|^2 = \sqrt{3}/9$ which in physical units leads to the definition of the maximum power as introduced in equation 3 of the main text. Using equation B5, we can then also determine the optimal detuning frequency for the steepest slope to

$$\tilde{\delta}_{\text{ss}} = -3|B|^2 - 1/\sqrt{12}. \quad (\text{B7})$$

In physical units the linear detuning at the steepest slope becomes $\Delta_{\text{opt}} \equiv \tilde{\delta}_{\text{ss}} \Gamma$ and thus as stated in the main text with the following equation

$$\Delta_{\text{opt}} = -\frac{3g_{\text{tot}} \kappa}{\Gamma^2} \frac{P_p}{\hbar \omega_p} - \frac{\Gamma}{\sqrt{12}}. \quad (\text{B8})$$

Using equation B6 and B7, it becomes clear that at the point of the steepest slope, we always have $|A|^2 = 3|B|^2$ and therefore also $\tilde{\delta} + |A|^2 = -1/\sqrt{12}$.

Appendix C: Sensitivity of the ring resonator

To determine the sensitivity of the system, we first analyze the output field of the resonator. Following [46, 47] and using the input-output theory with $b_{\text{out}} = \sqrt{\kappa} a_c - b_{\text{in}}$, we can then solve equation 1 for the steady state and derive the equation of the output-field b_{out} in dependency of the input field to

$$b_{\text{out}} = \left(\frac{\kappa}{\frac{1}{2} - i\Delta_{\text{tot}}} - 1 \right) b_{\text{in}}. \quad (\text{C1})$$

This equation is used to fit the measured transmission spectrum from Fig. 4. Using this equation C1 together with the dimensionless parameters from the equations B1-B3, we can derive the output power to

$$P_{\text{out}} = P_p \cdot \frac{\left(\frac{\kappa}{\Gamma} - \frac{1}{2} \right)^2 + \left(\tilde{\delta} + |A|^2 \right)^2}{\frac{1}{4} + \left(\tilde{\delta} + |A|^2 \right)^2}. \quad (\text{C2})$$

In a sensor application, the resonance condition and thus the detuning $\tilde{\delta}$ shifts due to external signal influences which represent basically a phase shift. Similar as in equation B3, we can introduce the phase shift $\phi = \delta \Delta / \Gamma$

and we can set $\tilde{\delta} \rightarrow \tilde{\delta} + \phi$, where ϕ originates from an externally induced phase shift or an externally induced temperature change with $\phi \sim \Delta T_{\text{ext}}$. Then, the sensitivity is defined by the linearization of equation C2 with respect to ϕ as $P_{\text{out}}(\phi) = P_{\text{out}}(0) + S\delta\Delta$ with

$$S = P_p \cdot G_{\text{geo}} G_{\text{det}} \left(1 + \frac{d}{d\phi} |A|^2 \right). \quad (\text{C3})$$

Thereby, G_{geo} describes the geometric gain with

$$G_{\text{geo}} = \frac{Q}{\omega_{R,T_0}} \left[\frac{1}{4} - \left(\frac{\kappa}{\Gamma} - \frac{1}{2} \right)^2 \right] \quad (\text{C4})$$

with the Q -factor of the ring resonator $Q = \omega_{R,T_0}/\Gamma$. The detuning gain G_{det} in equation C3 is given by

$$G_{\text{det}} = \frac{2(\tilde{\delta} + |A|^2)}{\left[(\tilde{\delta} + |A|^2)^2 + \frac{1}{4} \right]^2} \xrightarrow{\tilde{\delta} = \tilde{\delta}_{\text{ss}}} -\sqrt{27}. \quad (\text{C5})$$

It is clearly visible, that the best G_{geo} can be achieved with a high Q -factor and $\kappa/\Gamma = 1/2$, which is the case for the so called critical coupling of the ring resonator. To arrive at equation 4 of the main text, we finally have to show that $1+d|A|^2/d\phi$ reduces to $P_{\text{max}}/(P_{\text{max}} - P_p)$ at the optimal detuning $\tilde{\delta} = \tilde{\delta}_{\text{ss}}$. Therefore, we put $\tilde{\delta} = \tilde{\delta}_{\text{ss}} + \phi$ into equation (B4) and take the derivative with respect to ϕ to arrive at

$$\frac{d}{d\phi} |A|^2 = -\frac{2|B|^2 (\tilde{\delta}_{\text{ss}} + \phi + |A|^2)}{\left[(\tilde{\delta}_{\text{ss}} + \phi + |A|^2)^2 + \frac{1}{4} \right]^2} \cdot \left(1 + \frac{d}{d\phi} |A|^2 \right). \quad (\text{C6})$$

Next, we evaluate equation C6 at $\phi = 0$, exploit that $\tilde{\delta}_{\text{ss}} + |A|^2 = -1/\sqrt{12}$ and realize the relation $P_p/P_{\text{max}} = 9|B|^2/\sqrt{3}$ to arrive to equation 4 of the main text after a few more simple algebraic steps.

[1] K. J. Vahala, Optical microcavities, *Nature* **424**, 839 (2003).

[2] D. K. Armani, T. J. Kippenberg, S. M. Spillane, and K. J. Vahala, Ultra-high-Q toroid microcavity on a chip, *Nature* **421**, 925 (2003).

[3] P. Del'Haye, A. Schliesser, O. Arcizet, T. Wilken, R. Holzwarth, and T. J. Kippenberg, Optical frequency comb generation from a monolithic microresonator, *Nature* **450**, 1214 (2007).

[4] T. J. Kippenberg, R. Holzwarth, and S. A. Diddams, Microresonator-based optical frequency combs, *Science* **332**, 555 (2011).

[5] T. J. Kippenberg, A. L. Gaeta, M. Lipson, and M. L. Gorodetsky, Dissipative Kerr solitons in optical microresonators, *Science* **361** (2018).

[6] L. Chang, W. Xie, H. Shu, Q.-F. Yang, B. Shen, A. Boes, J. D. Peters, W. Jin, C. Xiang, S. Liu, G. Moille, S.-P. Yu, X. Wang, K. Srinivasan, S. B. Papp, K. Vahala, and J. E. Bowers, Ultra-efficient frequency comb generation in AlGaAs-on-insulator microresonators, *Nature Communications* **11**, 1331 (2020).

[7] N. L. Kazanskiy, S. N. Khonina, and M. A. Butt, A review of photonic sensors based on ring resonator structures: Three widely used platforms and implications of sensing applications, *Micromachines* **14**, 10.3390/mi14051080 (2023).

[8] S. Sbarra, B. Zabelich, M. Clementi, J. Liu, T. Kippenberg, and C.-S. Brès, UV, visible, and near-infrared light generation through cascaded nonlinear processes in silicon-nitride microring resonators pumped at telecom wavelength, in *Laser Resonators, Microresonators, and Beam Control XXVI*, Vol. 12871, edited by V. S. Ilchenko, A. M. Armani, and J. V. Sheldakova, International Society for Optics and Photonics (SPIE, 2024) p. 1287102.

[9] D. H. Geuzebroek and A. Driessens, Ring-resonator-based wavelength filters, in *Wavelength Filters in Fibre Optics*, edited by H. Venghaus (Springer Berlin Heidelberg, Berlin, Heidelberg, 2006) pp. 341–379.

[10] B. Little, S. Chu, H. Haus, J. Foresi, and J.-P. Laine, Microring resonator channel dropping filters, *Journal of Lightwave Technology* **15**, 998 (1997).

[11] L. Zhou and A. W. Poon, Electrically reconfigurable silicon microring resonator-based filter with waveguide-coupled feedback, *Opt. Express* **15**, 9194 (2007).

[12] A. Nordin, Optical-resonator-based biosensing systems: current status and future prospects, *Nanobiosensors in Disease Diagnosis* **Volume 5**, 41 (2016).

[13] K. Malmir, H. Habibian, and H. Ghafoorifard, Ultrasensitive optical biosensors based on microresonators with bent waveguides, *Optik* **216**, 164906 (2020).

[14] N. Toropov, G. Cabello, M. P. Serrano, R. R. Gutha, M. Rafti, and F. Vollmer, Review of biosensing with whispering-gallery mode lasers, *Light: Science & Applications* **10**, 42 (2021).

[15] Y.-T. Chen, Y.-C. Lee, Y.-H. Lai, J.-C. Lim, N.-T. Huang, C.-T. Lin, and J.-J. Huang, Review of integrated optical biosensors for point-of-care applications, *Biosensors (Basel)* **10**, 209 (2020).

[16] P. Tritschler, T. Ohms, A. Zimmermann, F. Zschocke, T. Strohm, and P. Degenfeld-Schonburg, Optical interferometer using two-mode squeezed light for enhanced chip-integrated quantum metrology (2024), arXiv:2309.10602 [quant-ph].

[17] P. Tritschler, T. Ohms, P. Degenfeld-Schonburg, F. Zschocke, and A. Zimmermann, Detection schemes for two-mode squeezed fiber optic sagnac interferometry, *IEEE Sensors Letters* **7**, 1 (2023).

[18] F. Dell'Olio, T. Tatoli, C. Ciminelli, and M. Armenise, Recent advances in miniaturized optical gyroscopes, *Journal of the European Optical Society - Rapid publications* **9** (2014).

[19] Z. Feng, Y. He, W. Yan, F. Yang, W. Han, and Z. Li, Progress of waveguide ring resonators used in micro-optical gyroscopes, *Photonics* **7**, 10.3390/photonics7040096 (2020).

[20] T. Amrane, J.-B. Jager, T. Jager, V. Calvo, and J.-M. Léger, Towards a fully integrated optical gyroscope using whispering gallery modes resonators, in *International Conference on Space Optics — ICSO 2014*, Vol. 10563, edited by Z. Sodnik, B. Cugny, and N. Karafolas, International Society for Optics and Photonics (SPIE, 2017) p. 105633Z.

[21] S. H. Nam and S. Yin, High-temperature sensing using whispering gallery mode resonance in bent optical fibers, *IEEE Photonics Technology Letters* **17**, 2391 (2005).

[22] G. Guan, S. Arnold, and M. Otugen, Temperature measurements using a micro-optical sensor based on whispering gallery modes, *Aiaa Journal - AIAA J* **44**, 2385 (2006).

[23] C. Zhang, G.-G. Kang, J. Wang, S. Wan, C.-H. Dong, Y.-J. Pan, and J.-F. Qu, Photonic thermometer by silicon nitride microring resonator with milli-kelvin self-heating effect, *Measurement* **188**, 110494 (2022).

[24] C.-H. Dong, L. He, Y.-F. Xiao, V. R. Gaddam, S. K. Ozdemir, Z.-F. Han, G.-C. Guo, and L. Yang, Fabrication of high-q polydimethylsiloxane optical microspheres for thermal sensing, *Applied Physics Letters* **94**, 231119 (2009).

[25] P. D. Drummond and D. F. Walls, Quantum theory of optical bistability. i. nonlinear polarisability model, *Journal of Physics A: Mathematical and General* **13**, 725 (1980).

[26] G. Duffing, *Erzwungene Schwingungen bei veränderlicher Eigenfrequenz und ihre technische Bedeutung* (F. Vieweg & Sohn Braunschweig, Braunschweig, 1918).

[27] I. D. Rukhlenko, M. Premaratne, and G. P. Agrawal, Analytical study of optical bistability in silicon ring resonators, *Opt. Lett.* **35**, 55 (2010).

[28] T. Carmon, L. Yang, and K. J. Vahala, Dynamical thermal behavior and thermal self-stability of microcavities, *Opt. Express* **12**, 4742 (2004).

[29] A. E. Fomin, M. L. Gorodetsky, I. S. Grudinin, and V. S. Ilchenko, Nonstationary nonlinear effects in optical microspheres, *J. Opt. Soc. Am. B* **22**, 459 (2005).

[30] T. Johnson, M. Borselli, and O. Painter, Self-induced optical modulation of the transmission through a high-q silicon microdisk resonator, *Optics express* **14**, 817 (2006).

[31] C. Schmidt, A. Chipouline, T. Pertsch, A. Tünnermann, O. Egorov, F. Lederer, and L. Deych, Nonlinear thermal effects in optical microspheres at different wavelength sweeping speeds, *Opt. Express* **16**, 6285 (2008).

[32] A. Arbabi and L. L. Goddard, Dynamics of self-heating in microring resonators, *IEEE Photonics Journal* **4**, 1702 (2012).

[33] X. Jiang and L. Yang, Optothermal dynamics in whispering-gallery microresonators, *Light: Science & Applications* **9**, 24 (2020).

[34] M. Novarese, S. R. Garcia, S. Cucco, D. Adams, J. Bovington, and M. Gioannini, Study of nonlinear effects and self-heating in a silicon microring resonator including a shockley-read-hall model for carrier recombination, *Opt. Express* **30**, 14341 (2022).

[35] V. I. Pavlov, N. M. Kondratiev, A. E. Shitikov, and V. E. Lobanov, Microresonator effective thermal parameters definition via thermal modes decomposition, *Photonics* **10**, 10.3390/photonics10101131 (2023).

[36] K. Ikeda, R. E. Saperstein, N. Alic, and Y. Fainman, Thermal and kerr nonlinear properties of plasma-deposited silicon nitride/silicon dioxide waveguides, *Opt. Express* **16**, 12987 (2008).

[37] S. Chen, L. Zhang, Y. Fei, and T. Cao, Bistability and self-pulsation phenomena in silicon microring resonators based on nonlinear optical effects, *Opt. Express* **20**, 7454 (2012).

[38] W. Bogaerts, P. De Heyn, T. Van Vaerenbergh, K. De Vos, S. Kumar Selvaraja, T. Claes, P. Dumon, P. Bienstman, D. Van Thourhout, and R. Baets, Silicon microring resonators, *Laser & Photonics Reviews* **6**, 47 (2012).

[39] C. J. Krückel, A. Fülöp, T. Klintberg, J. Bengtsson, P. A. Andrekson, and V. Torres-Company, Linear and nonlinear characterization of low-stress high-confinement silicon-rich nitride waveguides, *Opt. Express* **23**, 25827 (2015).

[40] A. M. Agarwal, L. Liao, J. S. Foresi, M. R. Black, X. Duan, and L. C. Kimerling, Low-loss polycrystalline silicon waveguides for silicon photonics, *Journal of Applied Physics* **80**, 6120 (1996).

[41] J. S. Levy, A. Gondarenko, M. A. Foster, A. C. Turner-Foster, A. L. Gaeta, and M. Lipson, Cmos-compatible multiple-wavelength oscillator for on-chip optical interconnects, *Nature Photonics* **4**, 37 (2010).

[42] H. A. Haus, *Waves and fields in optoelectronics*, Prentice-Hall series in solid state physical electronics (Prentice-Hall Englewood Cliffs, N.J., Englewood Cliffs, N.J., 1984).

[43] A. Yariv, Critical coupling and its control in optical waveguide-ring resonator systems, *IEEE Photonics Technology Letters* **14**, 483 (2002).

[44] T. Gu, M. Yu, D.-L. Kwong, and C. W. Wong, Molecular-absorption-induced thermal bistability in pecvd silicon nitride microring resonators, *Opt. Express* **22**, 18412 (2014).

[45] Z. Vernon and J. E. Sipe, Strongly driven nonlinear quantum optics in microring resonators, *Phys. Rev. A* **92**, 033840 (2015).

[46] M. J. Collett and C. W. Gardiner, Squeezing of intracavity and traveling-wave light fields produced in parametric amplification, *Phys. Rev. A* **30**, 1386 (1984).

[47] C. W. Gardiner and M. J. Collett, Input and output in damped quantum systems: Quantum stochastic differential equations and the master equation, *Phys. Rev. A* **31**, 3761 (1985).